

Feedback Design with VQ-VAE for Robust Precoding in Multi-User FDD Systems

Nurettin Turan *Graduate Student Member, IEEE*, Michael Baur *Graduate Student Member, IEEE*, Jianqing Li, and Wolfgang Utschick *Fellow, IEEE*

Abstract—In this letter, we propose a vector quantized-variational autoencoder (VQ-VAE)-based feedback scheme for robust precoder design in multi-user frequency division duplex (FDD) systems. We demonstrate how the VQ-VAE can be tailored to specific propagation environments, focusing on systems with low pilot overhead, which is crucial in massive multiple-input multiple-output (MIMO). Extensive simulations with real-world measurement data show that our proposed feedback scheme outperforms state-of-the-art autoencoder (AE)-based compression schemes and conventional Discrete Fourier transform (DFT) codebook-based schemes. These improvements enable the deployment of systems with fewer feedback bits or pilots.

Index Terms—Robust precoding, VQ-VAE, machine learning, feedback, measurement data.

I. INTRODUCTION

In the next generation of cellular communications systems (6G), the base station (BS) will have the capability to adapt to dynamic channel conditions. In massive MIMO FDD systems, this adaption is maintained by regular channel state information (CSI) feedback from the mobile terminals (MTs) due to the absence of channel reciprocity [1].

In this regard, conventional schemes entail estimating the downlink (DL) channel at the MTs and subsequently determining the feedback information using codebook-based schemes [1], [2]. In scenarios with spatial correlation due to specific antenna geometries, DFT-based codebooks are well-established and are part of 3rd Generation Partnership Project (3GPP) specifications [3], [4]. Alternatively, the feedback information can be obtained with state-of-the-art machine learning (ML)-based CSI compression schemes, e.g., [5]–[8]. In the seminal work [5], AEs were utilized for CSI feedback, where the encoder is used to compress at the MT side, and the decoder reconstructs at the BS side. Building on this concept, [6] introduced quantization in the AE’s latent space. In [7], VQ-VAEs were adopted to learn the quantization operation using an embedding in the latent space [9]. Moreover, [8], [10] explored the use of AEs for reconstructing channels from noisy input data, leveraging the denoising capabilities of AEs [11].

However, in massive MIMO FDD systems, where the BS is typically equipped with a high number of antennas, as many

The authors are with the TUM School of Computation, Information and Technology, Technische Universität München, 80333 Munich, Germany
Corresponding author: Nurettin Turan (e-mail: nurettin.turan@tum.de).

N. Turan and M. Baur contributed equally to this work. The authors acknowledge the financial support by the Federal Ministry of Education and Research of Germany in the program of “Souverän. Digital. Vernetzt.”. Joint project 6G-life, project identification number: 16KISK002. This work is funded by the Bavarian Ministry of Economic Affairs, Regional Development, and Energy as part of the project 6G Future Lab Bavaria.

©This work has been submitted to the IEEE for possible publication. Copyright may be transferred without notice, after which this version may no longer be accessible.

pilots as transmit antennas are required to be sent from the BS to the MTs to fully illuminate the channel. This results in a significant pilot overhead, which can be prohibitive [12]. In this work, in addition to noisy input data, system setups with fewer pilots than transmit antennas are considered, rendering the instantaneous reconstruction of the CSI particularly challenging. To address this, we propose a VQ-VAE-based feedback scheme for robust precoder design. The contributions of this work can be summarized as follows:

- We propose to utilize VQ-VAEs in combination with a state-of-the-art stochastic algorithm for robust precoder design in multi-user systems. To enhance the VQ-VAE training, we suggest adapting the loss function and the architecture based on model-based insights. Specifically, the covariance matrix at the VQ-VAE’s decoder output is constrained according to the array geometry at the BS side, a scalar embedding is employed, and the VQ-VAE input undergoes a pre-transformation.
- Due to the applied training procedure, the proposed scheme provides easy adaption to any desired signal-to-noise ratio (SNR) and supports multi-user operation for any number of MTs without requiring retraining.
- Extensive simulations using real-world measurement data demonstrate that the proposed feedback scheme for robust precoder design outperforms state-of-the-art AE-based compression schemes trained for instantaneous reconstruction, as well as conventional DFT codebook-based schemes. The performance improvements achieved with the proposed scheme enable the deployment of systems with fewer feedback bits or pilots.

II. SYSTEM MODEL AND CHANNEL DATA

A. Data Transmission Phase

We consider the DL of a single-cell multi-user system, where the BS equipped with N transmit antennas serves J single-antenna MTs. Linear precoding is adopted, with the precoded DL data vector given by $\mathbf{x} = \sum_{j=1}^J \mathbf{v}_j s_j$, where s_j is the transmit signal for MT j , $E[s_j] = 0$, $E[|s_j|^2] = 1$, and $\mathbf{v}_j \in \mathbb{C}^N$ is the precoding vector of MT j . The precoders satisfy the transmit power constraint $\sum_{j=1}^J \text{tr}(\mathbf{v}_j^H \mathbf{v}_j) = \rho$. The sum-rate is expressed as

$$R = \sum_{j=1}^J \log_2 \left(1 + \frac{|\mathbf{h}_j^T \mathbf{v}_j|^2}{\sum_{j' \neq j} |\mathbf{h}_j^T \mathbf{v}_{j'}|^2 + \sigma_n^2} \right), \quad (1)$$

where $\mathbf{h}_j \in \mathbb{C}^N$ denotes the channel of MT j and σ_n^2 is the noise variance. In the considered FDD system, the BS designs

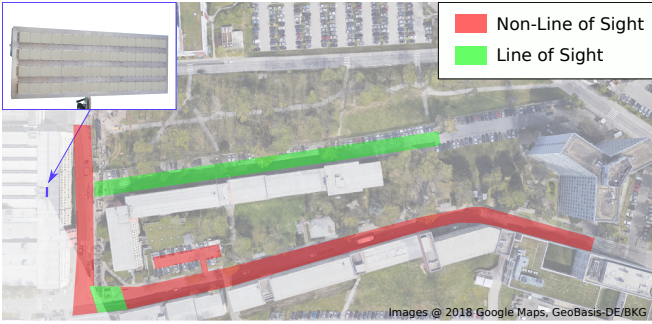


Fig. 1: Measurement campus in Stuttgart, Germany [14].

the precoders \mathbf{v}_j based on each MT's feedback information, which is encoded by B bits.

B. Pilot Transmission Phase

Before data transmission, n_p orthogonal pilots are broadcasted to all MTs, allowing each MT to infer its feedback information. During the pilot transmission phase, the received signal $\mathbf{y}_j \in \mathbb{C}^{n_p}$ of each MT is given by

$$\mathbf{y}_j = \mathbf{P}\mathbf{h}_j + \mathbf{n}_j \quad (2)$$

where $\mathbf{n}_j \sim \mathcal{N}_{\mathbb{C}}(\mathbf{0}, \mathbf{\Sigma})$ represents the additive white Gaussian noise (AWGN) with $\mathbf{\Sigma} = \sigma_n^2 \mathbf{I}_{n_p}$. We utilize a 2D-DFT (sub)matrix as the pilot matrix \mathbf{P} , which is motivated by the uniform rectangular array (URA) at the BS, cf. [13]. To meet the power constraint, each column \mathbf{p}_ℓ of \mathbf{P}^T is normalized such that $\|\mathbf{p}_\ell\|_2^2 = \rho$ for all $\ell \in \{1, 2, \dots, n_p\}$. We consider systems with fewer pilots than transmit antennas, i.e., $n_p < N$.

C. Real-World Channel Data

The measurement campaign took place at the Nokia campus in Stuttgart, Germany, in 2017. As shown in Fig. 1, the BS antenna, with a 10° down-tilt, was installed on a rooftop approximately 20 m above the ground. The antenna array geometry was tailored to the urban microcell (UMi) propagation scenario. Thus, the BS comprises a URA with $N_v = 4$ vertical and $N_h = 16$ horizontal single polarized patch antennas, totaling $N = 64$ elements. The horizontal spacing was $\lambda/2$, and the vertical spacing was λ , where λ is the wavelength. The carrier frequency used was 2.18 GHz. The single monopole receive antenna, representing the MTs, was mounted on a vehicle at a height of 1.5 m, which moved at a maximum speed of 25 kmph. Further details can be found in [14].

III. PROPOSED VQ-VAE-BASED FEEDBACK SCHEME FOR ROBUST PRECODER DESIGN

In general, the VQ-VAE's loss function is given by, cf. [9],

$$\mathcal{L}_{\text{VQ-VAE}} = \mathcal{L}_{\text{rec}} + \|\text{sg}(\mathbf{z}_j) - \mathbf{f}_j\|_2^2 + \beta \|\mathbf{z}_j - \text{sg}(\mathbf{f}_j)\|_2^2, \quad (3)$$

where \mathcal{L}_{rec} denotes the reconstruction loss and $\text{sg}(\cdot)$ denotes the stop gradient operator, which treats its argument as a constant. The second term in (3) is the dictionary learning term, which ensures that the embedding \mathcal{E} is learned such that the output after quantization, i.e., \mathbf{f}_j is as close as possible to

the unquantized latent representation \mathbf{z}_j . The third term in (3) is the commitment loss, encouraging the encoder to commit to the embedding \mathcal{E} and ensuring that the encoder output does not grow unbounded. The balancing hyper-parameter $\beta = 0.25$ is introduced to facilitate a good reconstruction by weighting the commitment loss lower and thereby enhancing the impact of the dictionary learning [7], [9]. To maintain a continuous gradient flow between the encoder and decoder, despite the discontinuity introduced by quantization, the gradients from the decoder input to the encoder output are copied using $\mathbf{f}_j = \mathbf{z}_j + \text{sg}(\mathbf{f}_j - \mathbf{z}_j)$. In summary, the encoder is trained using the first and third terms of the loss (3), the embedding \mathcal{E} is learned through the second term, and the decoder is trained with the first term.

The VQ-VAE can be tailored to the BS environment characteristics to enable robust precoder design as follows. We require the VQ-VAE to output a mean vector $\boldsymbol{\mu}_j$, and another vector \mathbf{c}_j parametrizing a covariance matrix as approximate statistical information about the channel \mathbf{h}_j (see Fig. 2). Since we have a URA deployed at the BS side, a reasonable choice is to constrain the covariance matrices to be block-Toeplitz matrices with Toeplitz blocks:

$$\mathbf{C}_j = \mathbf{Q}^H \text{diag}(\mathbf{c}_j) \mathbf{Q} \quad (4)$$

with $\mathbf{Q} = \mathbf{Q}_{N_v} \otimes \mathbf{Q}_{N_h}$, where \mathbf{Q}_T (with $T \in \{N_v, N_h\}$) contains the first T columns of a $2T \times 2T$ DFT matrix and $\mathbf{c}_j \in \mathbb{R}_+^{4N}$, see [15]. Consequently, the covariance matrices are fully characterized by the output vectors \mathbf{c}_j . This structural constraint acts as a regularization and helps to decrease the model parameters since the decoder output vector \mathbf{c}_j fully determines the covariance matrix \mathbf{C}_j .

We adopt a similar encoder and decoder architecture as in [15], where we adapt the input and latent dimension accordingly. We also adopt an embedding \mathcal{E} consisting of in total C scalar entries, i.e., $\mathcal{E} = \{e_1, e_2, \dots, e_C\}$, keeping in mind that also the embedding needs to be shared with the MTs. For a fixed latent space dimension N_L , the i -th entry of the feedback vector \mathbf{f}_j is obtained by using the embedding \mathcal{E} as

$$f_{j,i} = \min_{e_c \in \mathcal{E}} |e_c - z_{j,i}|, \quad (5)$$

where $z_{j,i}$ denotes the i -th entry of the unquantized latent representation \mathbf{z}_j , and $i = 1, \dots, N_L$. In this way, the feedback vector \mathbf{f}_j can be fully described by $B = N_L \log_2 C$ bits. In principle, sub-chunks of \mathbf{z}_j could be quantized with vectors instead of scalars, see [9]. However, in our simulations, we did not observe any gains with an embedding consisting of vectors of relatively low dimensions instead of scalars. With vectors of too large dimensions, the training procedure is even infeasible if a feedback size of tens to hundreds of bits is desired.

The observation in (2) is first multiplied with the pilot matrix to obtain a coarse estimate. Subsequently, we apply \mathbf{Q} as a transformation, which is inspired by [16] and can be interpreted as an angular domain transformation, cf., e.g., [5]. Accordingly, the input to the VQ-VAE is given by $\mathbf{Q}\mathbf{P}^H \mathbf{y}_j$.

Taking into account the adaptations to tailor the VQ-VAE for robust precoder design for a specific BS environment, the

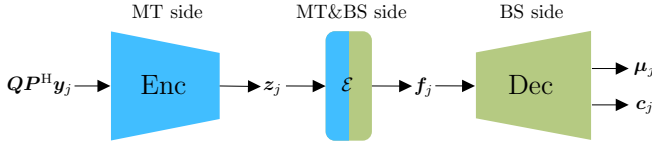


Fig. 2: Structure of the proposed VQ-VAE for robust precoder design.

overall loss function is the loss from (3) using the embedding $\mathcal{E} = \{e_1, e_2, \dots, e_C\}$ with the reconstruction loss

$$\mathcal{L}_{\text{rec}} = \log \det(\pi \mathbf{C}_j) + (\mathbf{h}_j - \boldsymbol{\mu}_j)^H \mathbf{C}_j^{-1} (\mathbf{h}_j - \boldsymbol{\mu}_j). \quad (6)$$

Multi-user operation for any desired number of MTs J is supported since the VQ-VAE is trained to allow the inference of statistical information about the channel of any MT within the BS cell environment. To enable operation at different SNR levels, we train the VQ-VAE for an SNR range from 0 to 20 dB. In particular, for the offline training, we utilize the training set $\{\mathbf{h}^{(m)}\}_{m=1}^M$ and generate correspondingly encoder inputs $\mathbf{Q}\mathbf{P}^H \mathbf{y}^{(m)}$ according to (2) where we randomly draw a noise variance to obtain an SNR from the range specified above.

In Fig. 2, the VQ-VAE with the proposed adaptations is depicted. As discussed before, knowledge of the encoder and the embedding is required to enable the MTs to infer their feedback information. In the online phase, given the observation \mathbf{y}_j at each MT j , the observation is preprocessed, passed through the encoder to obtain the unquantized latent variable \mathbf{z}_j , and finally quantized using the embedding \mathcal{E} to obtain the feedback information vector \mathbf{f}_j . Each MT j sends the feedback information encoded with $N_L \log_2 C$ bits back to the BS. At the BS side, the acquired statistical information about each MT is used in the following way to design precoders.

We utilize the sample generation capabilities of VQ-VAEs, treating the MT channels as random variables, and apply a stochastic version of the well-known iterative weighted minimum mean square error (WMMSE) algorithm [17], specifically the stochastic WMMSE (SWMMSE) algorithm from [18] for robust precoder design. In each iteration step, the SWMMSE requires samples that follow the channel distribution of each MT. Therefore, based on each MT's feedback information, we propose generating samples using the VQ-VAE as

$$\tilde{\mathbf{h}}_j \sim \mathcal{N}_{\mathbb{C}}(\boldsymbol{\mu}_j, \mathbf{C}_j), \quad (7)$$

resembling samples from the channel distribution of MT j . The BS uses the generated samples in each iteration step of the SWMMSE algorithm to jointly design the precoders for all MTs. A summary of the proposed VQ-VAE-based feedback scheme for robust precoder design is provided in Algorithm 1.

IV. BASELINE FEEDBACK SCHEMES FOR PRECODING

A. State-of-the-art AE and VQ-VAE-based Feedback Schemes

In state-of-the-art feedback schemes involving AEs or VQ-VAEs, a reconstruction $\hat{\mathbf{h}}_j$ of the channel of MT j is obtained at the decoder output, cf. [5], [7]. To facilitate a fair comparison, we utilize the same VQ-VAE architecture, encoder input pre-processing, and an embedding \mathcal{E} of the same size. The main adaptation is thus given by the decoder output, where the output covariance is fixed to be the identity and only a mean

Algorithm 1 VQ-VAE-based Feedback Scheme for Robust Precoder Design

Require: Offline trained VQ-VAE where encoder (Enc) and embedding \mathcal{E} are available at the MTs and decoder (Dec) and embedding \mathcal{E} are available at the BS.

Feedback Inference at the MTs

- 1: Infer unquantized latent \mathbf{z}_j from preprocessed observation at each MT j
 $\mathbf{z}_j = \text{Enc}(\mathbf{Q}\mathbf{P}^H \mathbf{y}_j) \forall j$
- 2: Obtain quantized latent representation \mathbf{f}_j at each MT j
 $f_{j,i} = \min_{e_c \in \mathcal{E}} |e_c - z_{j,i}|$ with $i = 1, \dots, N_L \forall j$
- 3: Each MT j feeds back \mathbf{f}_j encoded by $B = N_L \log_2 C$ bits

Robust Precoder Design at the BS

- 4: Obtain statistical description of each MT j
 $(\boldsymbol{\mu}_j, \mathbf{C}_j) = \text{Dec}(\mathbf{f}_j) \forall j$
- 5: Compute covariance matrix \mathbf{C}_j for each MT j
 $\mathbf{C}_j = \mathbf{Q}^H \text{diag}(\mathbf{c}_j) \mathbf{Q} \forall j$
- 6: Provide statistics of each MT j for sampling in the SWMMSE algorithm and obtain precoders
 $\{\mathbf{v}_j\}_j^J \leftarrow \text{SWMMSE}(\{\tilde{\mathbf{h}}_j \sim \mathcal{N}_{\mathbb{C}}(\boldsymbol{\mu}_j, \mathbf{C}_j)\}_{j=1}^J)$

vector, denoted by $\tilde{\mathbf{h}}_j$, is inferred. Accordingly, the overall loss function which aims to reconstruct the instantaneous channel is the loss from (3) with the mean squared error (MSE) as reconstruction loss

$$\mathcal{L}_{\text{rec}} = \|\mathbf{h}_j - \tilde{\mathbf{h}}_j\|_2^2. \quad (8)$$

In the case of the regular AE, the embedding is omitted, and the overall loss degenerates to the MSE reconstruction loss. Also, in these cases, multi-user operation for any desired number of MTs J is supported, and we train for the same SNR range to facilitate operation for different SNR levels. Since the information about each MT j is a reconstruction $\tilde{\mathbf{h}}_j$, we apply the iterative WMMSE algorithm for precoder design. Specifically, we use [19, Algorithm 1].

B. Conventional DFT Codebook-based Feedback Scheme

In conventional codebook-based feedback schemes, each MT first computes a channel estimate $\hat{\mathbf{h}}_j$ and then determines the channel directional information as (see, e.g., [2]):

$$k_j^* = \arg \max_k |\mathbf{c}_k^H \hat{\mathbf{h}}_j| \quad (9)$$

where $\mathbf{c}_k \in \mathcal{C}$, with the codebook $\mathcal{C} = \{\mathbf{c}_1, \dots, \mathbf{c}_{K_{\text{Dir}}}\}$ of cardinality $|\mathcal{C}| = K_{\text{Dir}} = 2^{B_{\text{Dir}}}$ with B_{Dir} bits. Since we have a URA at the BS, a 2D-DFT codebook is used, which is constructed by the Kronecker product of two under-/oversampled DFT matrices [3]. The under-/oversampling factors are chosen to satisfy $|\mathcal{C}| = K_{\text{Dir}} = 2^{B_{\text{Dir}}}$ for a given B_{Dir} . Furthermore, the channel magnitude information m_j is assumed to be the norm of the estimated channel $\hat{\mathbf{h}}_j$ and is encoded using B_{Mag} bits [2]. Thus, the overall feedback information is encoded using $B = B_{\text{Dir}} + B_{\text{Mag}}$ bits. Based on the feedback from each MT, the BS represents the channel of each MT as [2],

$$\hat{\mathbf{h}}_j^{(q)} = m_j \mathbf{c}_{k_j^*}, \quad (10)$$

and then utilizes the iterative WMMSE [19, Algorithm 1] to jointly design the precoders.

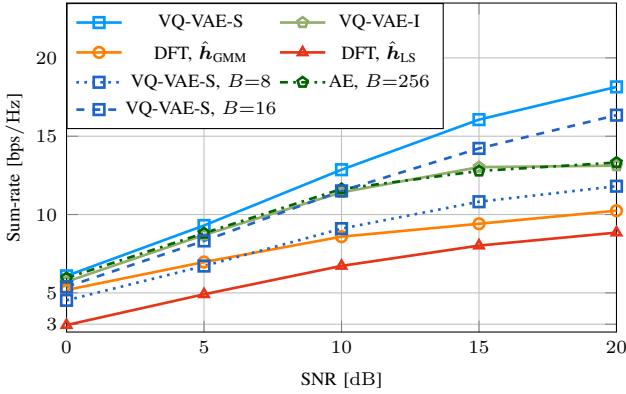


Fig. 3: The sum-rate over the SNR for a system with $B = 40$ feedback bits, $J = 8$ MTs, and $n_p = 8$ pilots.

V. SIMULATION RESULTS

We use 420,000 measurement data samples from the measurement campaign detailed in Section II-C. Specifically, $M = 400,000$ samples are used for training the data-based methods, 10,000 for validation, and 10,000 for evaluation. The data samples are normalized such that $E[\|\mathbf{h}\|^2] = N$. Additionally, we set $\rho = 1$, allowing the SNR to be defined as $\frac{1}{\sigma_n^2}$. The sum-rate averaged over 500 multi-user constellations is employed as the performance metric, where J MTs are randomly selected from our evaluation set for each constellation. For the SWMMSE as well as the iterative WMMSE, we set the maximum number of iterations to $I_{\max} = 300$. For clarity, we omit the index j in the subsequent descriptions.

In the following discussion, the proposed VQ-VAE-based feedback scheme from Section III, which utilizes statistical information for precoder design, is denoted by “VQ-VAE-S.” The baseline VQ-VAE feedback scheme from Section IV-A, which uses the instantaneous reconstructions, is denoted by “VQ-VAE-I,” and the regular AE with no quantization in the latent space by “AE.” As outlined in Section IV-B, the DFT codebook-based feedback scheme requires channel estimation. We consider two estimators: the Gaussian mixture model (GMM)-based channel estimator $\hat{\mathbf{h}}_{\text{GMM}}$ with 64 components [20] and the conventional least squares (LS) estimator $\hat{\mathbf{h}}_{\text{LS}}$. Cases where channel estimation is performed at each MT and the feedback information is then determined using the DFT codebook-based scheme are denoted as “DFT, $\{\hat{\mathbf{h}}_{\text{GMM}}, \hat{\mathbf{h}}_{\text{LS}}\}$.”

In the subsequent simulations, we fix the feedback budget to $B = 40$ bits, if not mentioned otherwise. This is motivated by a typical compression ratio for the regular AE with $N_L = 8$, cf. [5], where each latent entry is described by 32 bits (single precision), yielding $8 \cdot 32 = 256$ bits in total (“AE, $B=256$ ”). We observed, by introducing the embedding with as few as $C = 32$ (i.e. 5 bits per entry), the same performance was achieved with the “VQ-VAE-I,” see Fig. 3. For the VQ-VAE based methods “VQ-VAE-S” and “VQ-VAE-I,” we thus fix $N_L = 8$ and set $C = 32$ ($N_L \log_2 C = 8 \cdot 5 = 40$ bits). For the DFT codebook-based scheme we allocate $B_{\text{Dir}} = 8$ bits for the directional information and $B_{\text{Mag}} = 32$ bits for the magnitude (single precision), ensuring $B_{\text{Dir}} + B_{\text{Mag}} = 40$ bits. While different bit allocations for B_{Dir} and B_{Mag} are possible to achieve a total of $B = 40$ bits, the chosen

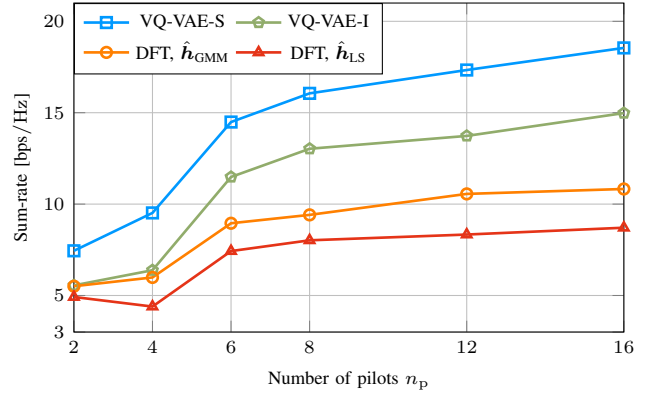


Fig. 4: The sum-rate over the number of pilots n_p for a system with $J = 8$ MTs, $B = 40$ feedback bits, and $\text{SNR} = 15$ dB.

allocation maintains reasonable complexity for determining channel directional information. Additionally, the “VQ-VAE-I” method inherently aims for a more efficient bit allocation for improved instantaneous reconstruction compared to the conventional DFT codebook-based scheme.

In Fig. 3, we have $J = 8$ MTs and $n_p = 8$ pilots and depict the sum-rate over the SNR. The proposed scheme “VQ-VAE-S” performs best, followed by the “VQ-VAE-I.” The conventional approaches “DFT, $\{\hat{\mathbf{h}}_{\text{GMM}}, \hat{\mathbf{h}}_{\text{LS}}\}$ ” perform poorly, especially at high SNR levels. Despite improvements with the GMM estimator over the LS estimator, the performance remains poor due to significant channel estimation errors. Our proposed scheme with even a reduced feedback bit overhead “VQ-VAE-S, $B = 16$ ” ($N_L = 8$, $C = 4$) performs comparable to the “VQ-VAE-I” approach with $B = 40$ bits in the low SNR regime, and is superior for high SNR levels. The proposed scheme with only 8 feedback bits denoted by “VQ-VAE-S, $B = 8$ ” ($N_L = 8$, $C = 2$) significantly outperforms “DFT, $\hat{\mathbf{h}}_{\text{LS}}$ ” and performs comparable to “DFT, $\hat{\mathbf{h}}_{\text{GMM}}$ ” in the low SNR regime, and is superior for high SNR levels. Accordingly, the performance gains from the proposed VQ-VAE-based robust precoder design scheme allow for deploying systems with reduced feedback overhead while maintaining performance.

In Fig. 4, we examine the impact of the number of pilots n_p on the performance with $J = 8$ MTs for a fixed SNR of 15 dB. The proposed scheme “VQ-VAE-S” performs best for all considered numbers of pilots n_p . With only $n_p = 6$ pilots, the “VQ-VAE-S” approach performs almost as well as the “VQ-VAE-I” baseline with $n_p = 16$ pilots. Additionally, with $n_p = 4$ pilots, the “VQ-VAE-S” approach performs almost as well as the “DFT, $\hat{\mathbf{h}}_{\text{GMM}}$ ” approach and outperforms “DFT, $\hat{\mathbf{h}}_{\text{LS}}$ ” each with $n_p = 16$ pilots. This analysis reveals that systems with lower pilot overhead can be deployed without sacrificing performance compared to the baseline schemes.

In Fig. 5, we set $n_p = 8$ pilots, and $\text{SNR} = 15$ dB and vary the number J of served MTs. It can be seen that the VQ-VAE-based feedback scheme “VQ-VAE-S” is superior as compared to the baselines for all numbers of MTs except for a setup with only two MTs. Remarkably, the sum-rate of the “VQ-VAE-S” approach steadily increases with an increasing number of MTs. The remaining approaches exhibit saturation or even slightly degrade with an increasing number of MTs. This can be reasoned by the fact that with an increasing

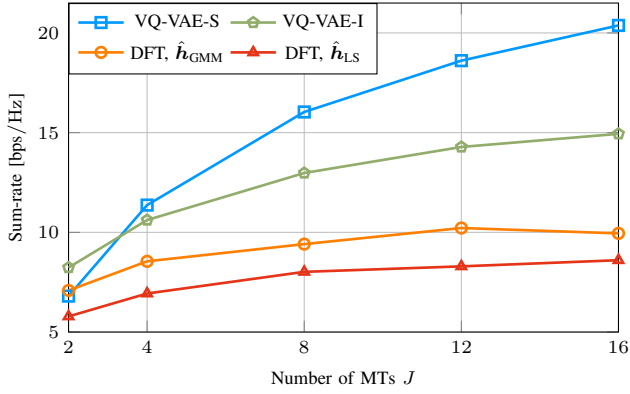


Fig. 5: The sum-rate over the number of MTs J for a system with $B = 40$ feedback bits, $n_p = 8$ pilots, and $\text{SNR} = 15$ dB.

number of MTs, resolving the interference present in the scenario becomes more difficult, particularly when restricted to a directional codebook of finite size. In contrast, with the proposed robust approach “VQ-VAE-S,” due to the involved sampling procedure (see Algorithm 1), a different representative interference scenario is provided to and exploited by the SWMMSE to design the precoders. For a system with only two MTs, the interference is less severe, and thus, the “VQ-VAE-I” aiming for an instantaneous reconstruction is beneficial.

Lastly, in Fig. 6, we set $J = 8$ MTs, $n_p = 8$ pilots, and $\text{SNR} = 15$ dB and investigate the impact of the number B of feedback bits on the system performance for the two SNR levels 10 dB and 20 dB. For $B \leq 40$, we adopt $N_L = 8$ and correspondingly $C \in \{2, 4, 8, 32\}$ (i.e. $\{1, 2, 3, 5\}$ bits per entry). For $B \geq 64$, we adopt $N_L = 32$ and $C \in \{4, 16\}$ (i.e. $\{2, 4\}$ bits per entry). The proposed scheme “VQ-VAE-S” outperforms the baseline “VQ-VAE-I” for all feedback bit configurations by a large margin, especially for $\text{SNR} = 20$ dB. Once again, the results indicate that the proposed scheme “VQ-VAE-S” can achieve superior performance than the baseline approach “VQ-VAE-I” with fewer bits, reducing both feedback overhead and processing requirements at the MTs.

VI. CONCLUSION

In this letter, we proposed a VQ-VAE-based feedback scheme for robust precoder design in multi-user FDD systems. The VQ-VAE can be tailored to the characteristics of the propagation environment and outperformed conventional DFT codebook-based and state-of-the-art AE-based feedback schemes in systems characterized by low pilot overhead. Future work can enhance the proposed VQ-VAE-based feedback scheme by embedding it into an end-to-end system that learns both the pilot matrix and the precoder optimization.

REFERENCES

- [1] D. J. Love, R. W. Heath, V. K. N. Lau, D. Gesbert, B. D. Rao, and M. Andrews, “An overview of limited feedback in wireless communication systems,” *IEEE J. Sel. Areas Commun.*, vol. 26, no. 8, pp. 1341–1365, 2008.
- [2] F. Kaltenberger, M. Kountouris, D. Gesbert, and R. Knopp, “On the trade-off between feedback and capacity in measured MU-MIMO channels,” *IEEE Trans. Wireless Commun.*, vol. 8, no. 9, pp. 4866–4875, 2009.
- [3] J. Li, X. Su, J. Zeng, Y. Zhao, S. Yu, L. Xiao, and X. Xu, “Codebook design for uniform rectangular arrays of massive antennas,” in *IEEE 77th Veh. Technol. Conf.*, 2013, pp. 1–5.

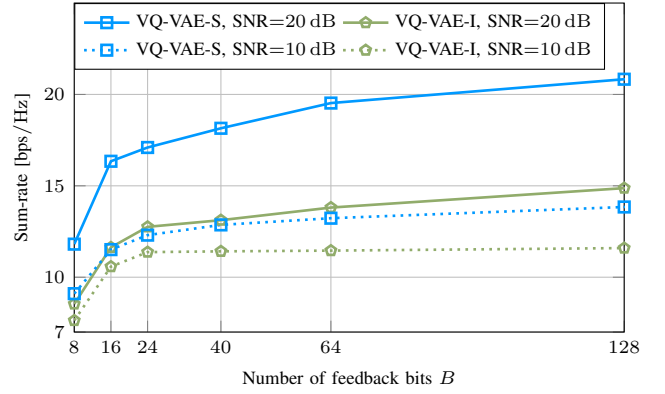


Fig. 6: The sum-rate over the number of feedback bits B , for a system with $J = 8$ MTs, $n_p = 8$ pilots, and $\text{SNR} \in \{10 \text{ dB}, 20 \text{ dB}\}$.

- [4] 3GPP, “NR; Physical channels and modulation,” 3rd Generation Partnership Project (3GPP), Tech. Spec. 38.211 (V18.0.0), Sep. 2023.
- [5] C.-K. Wen, W.-T. Shih, and S. Jin, “Deep learning for massive MIMO CSI feedback,” *IEEE Wireless Commun. Lett.*, vol. 7, no. 5, pp. 748–751, 2018.
- [6] J. Guo, C.-K. Wen, S. Jin, and G. Y. Li, “Convolutional neural network-based multiple-rate compressive sensing for massive MIMO CSI feedback: Design, simulation, and analysis,” *IEEE Trans. Wireless Commun.*, vol. 19, no. 4, pp. 2827–2840, 2020.
- [7] V. Rizzello, M. Nerini, M. Joham, B. Clerckx, and W. Utschick, “User-driven adaptive CSI feedback with ordered vector quantization,” *IEEE Wireless Commun. Lett.*, vol. 12, no. 11, pp. 1956–1960, 2023.
- [8] A. Lee, H. Park, Y. Kwon, H. Lee, and S. Chong, “Practical denoising autoencoder for CSI feedback without clean target in massive MIMO networks,” *IEEE Wireless Commun. Lett.*, vol. 13, no. 2, pp. 525–529, 2024.
- [9] A. van den Oord, O. Vinyals, and K. Kavukcuoglu, “Neural discrete representation learning,” in *Proc. Adv. Neural Inf. Process. Syst.*, vol. 30, 2017, p. 6306–6315.
- [10] V. Rizzello and W. Utschick, “Learning the CSI denoising and feedback without supervision,” in *IEEE 22nd Int. Workshop Signal Process. Adv. Wireless Commun. (SPAWC)*, 2021, pp. 16–20.
- [11] P. Vincent, H. Larochelle, Y. Bengio, and P.-A. Manzagol, “Extracting and composing robust features with denoising autoencoders,” in *Proc. 25th Int. Conf. Mach. Learn.*, ser. ICML ’08. New York, NY, USA: Association for Computing Machinery, 2008, p. 1096–1103.
- [12] E. Björnson, E. G. Larsson, and T. L. Marzetta, “Massive MIMO: ten myths and one critical question,” *IEEE Commun. Mag.*, vol. 54, no. 2, pp. 114–123, 2016.
- [13] Y. Tsai, L. Zheng, and X. Wang, “Millimeter-wave beamformed full-dimensional MIMO channel estimation based on atomic norm minimization,” *IEEE Trans. Commun.*, vol. 66, no. 12, pp. 6150–6163, 2018.
- [14] C. Hellings, A. Dehmani, S. Wesemann, M. Koller, and W. Utschick, “Evaluation of neural-network-based channel estimators using measurement data,” in *Proc. Int. ITG Workshop on Smart Antennas*, 2019, pp. 1–5.
- [15] M. Baur, B. Böck, N. Turan, and W. Utschick, “Variational autoencoder for channel estimation: Real-world measurement insights,” in *27th Int. Workshop Smart Antennas*, 2024, pp. 117–122.
- [16] D. Neumann, T. Wiese, and W. Utschick, “Learning the MMSE channel estimator,” *IEEE Trans. Signal Process.*, vol. 66, no. 11, pp. 2905–2917, Jun. 2018.
- [17] Q. Shi, M. Razaviyayn, Z.-Q. Luo, and C. He, “An iteratively weighted MMSE approach to distributed sum-utility maximization for a MIMO interfering broadcast channel,” *IEEE Trans. Signal Process.*, vol. 59, no. 9, pp. 4331–4340, 2011.
- [18] M. Razaviyayn, M. Sanjabi, and Z.-Q. Luo, “A stochastic successive minimization method for nonsmooth nonconvex optimization with applications to transceiver design in wireless communication networks,” *Math. Program.*, vol. 157, no. 2, p. 515–545, 2016.
- [19] Q. Hu, Y. Cai, Q. Shi, K. Xu, G. Yu, and Z. Ding, “Iterative algorithm induced deep-unfolding neural networks: Precoding design for multiuser MIMO systems,” *IEEE Trans. Wireless Commun.*, vol. 20, no. 2, pp. 1394–1410, 2021.
- [20] M. Koller, B. Fesl, N. Turan, and W. Utschick, “An asymptotically MSE-optimal estimator based on Gaussian mixture models,” *IEEE Trans. Signal Process.*, vol. 70, pp. 4109–4123, 2022.